Supporting Information

Cobalt-Polypyrrole/Melamine-Derived Co-N@NC Catalysts for Efficient Base-Free Formic Acid Dehydrogenation and Formylation of Quinolines through Transfer Hydrogenation

Yan Leng[a,*,‡], *Shengyu Du*[a,‡], *Guodong Feng*[c,‡], *Xinxin Sang*[a], *Pingping Jiang*[a], *Hui Li*[b*], *Dawei Wang*[a]

a. School of Chemical and Material Engineering, Jiangnan University, Wuxi, Jiangsu, 214122, China. E-mail: yanleng@jiangnan.edu.cn.

b. School of Pharmaceutical Science, Jiangnan University, Wuxi, Jiangsu 214122, China. E-mail: lihui@jiangnan.edu.cn.

Materials and Methods

Pyrrole, dimethoxymethane, iron(III) chloride, 1,2-dichloroethane, $Co(OAc)_2$, and methanol were purchased from Shanghai Chemical Reagent. Unless otherwise stated, all solvents and chemicals used were of commercially available analytical grade and used without further treatment.

Scanning electron microscopy (SEM) images were performed on a SUPERSCAN SSX-550 electron microscope. Transmission electron microscopy (TEM) images were recorded with a Tecnai G2 F30 S-Twin electron microscope. Energy-dispersive X-ray spectrometry (EDS) analysis and elemental mapping were obtained on this instrument (accelerated voltage: 20 kV). The nitrogen sorption isotherms and pore size distribution curves were measured at the liquid nitrogen temperature (77 K) using a BELSORP-MINI analyzer. XRD patterns were collected on the Bruker D8 Advance powder diffractometer using Ni-filtered Cu/Kα radiation source at 40 kV and 20 mA, from 5 ° to 90 ° with a scan rate of 2 °/min. Raman analysis was performed on a PerkinElmer-Raman Station 400F spectrometer equipped with a liquid N_2 cooled charge-coupled device detector and a confocal microscope. A 350 mW near-infrared 785 nm laser was used for analysis under ambient conditions. TGA was performed on a STA409 instrument in O_2 at a heating rate of 10 °C/min. Inductively coupled plasma atomic emission spectroscopy (ICP-AES) analysis for Co loading amount was determined by a Jarrell-Ash 1100 ICP-AES spectrometer. FT-IR spectra were carried out with a Nicolet 360 FT-IR instrument (KBr discs) in the 4000-400 cm^{-1} region. X-ray photoelectron spectroscopy (XPS) was conducted on a PHI 5000 Versa Probe X-ray photoelectron spectrometer equipped with Al-Ka radiation (1486.6 eV). XAFS spectrum at the Co K-edge (7709 eV) was measured at the BL14W1 beamline

station of the Beijing Synchrotron Radiation Facility, China. The Co K-edge XANES data were recorded in a transmission mode, Co foil was used as a reference. H_2-TPR analysis was measured on a ChemiSorb 2720 TPx chemisorption analyzer. 0.1 g sample was pretreated under Ar flow (40 mL/min) at 150 °C for 90 min, and then the sample was cooled down to 30 °C in an Ar flow. Afterwards, the temperature programmed reduction process was conducted in a flow of 10% H_2/Ar (40 mL/min) up to 800 °C at a heating rate of 10 °C/min. 1H NMR spectra were measured with a Bruker DPX 4 spectrometer at ambient temperature in $CDCl_3$ using TMS as the internal reference. The high-angle annular dark-filed scanning TEM (HAADF-STEM) images were performed on a Talos F200X instrument.

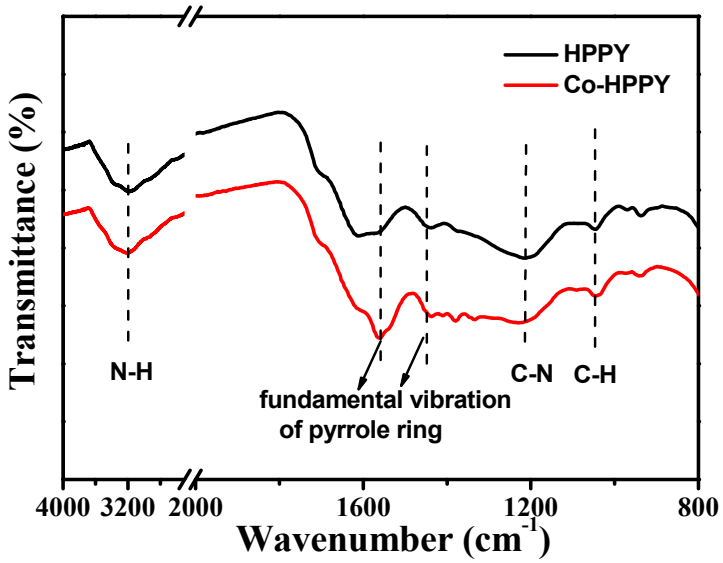

Figure S1. FT-IR spectra of HPPY and Co-HPPY.

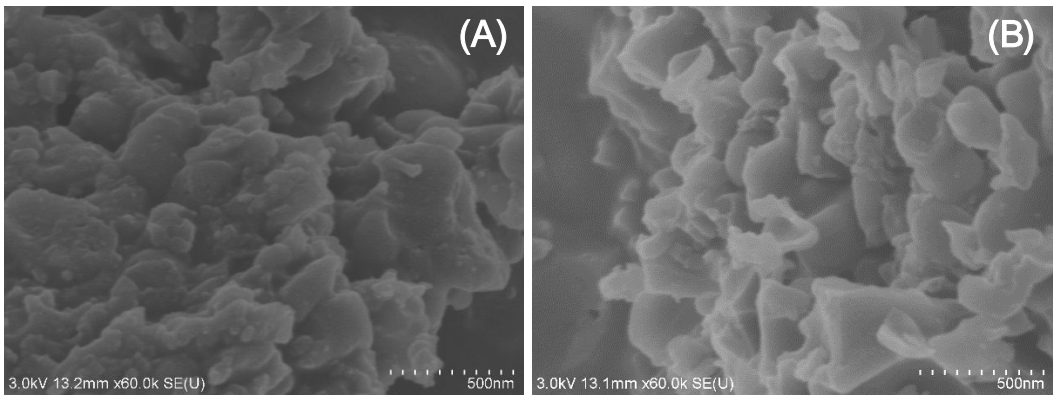

Figure S2. SEM images for (A) Co-HPPY and (B) $(Co\text{-}N)_{6.8}$@NC.

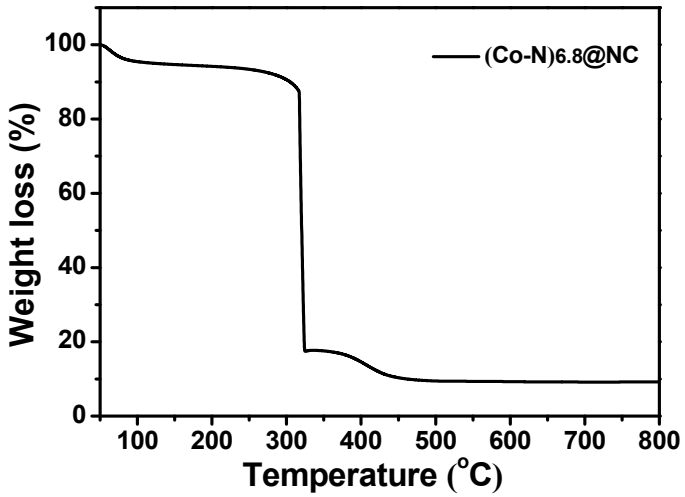

Figure S3. TGA curve for $(Co\text{-}N)_{6.8}$@NC in O_2.

Table S1 Chemical composition of N-doped carbon catalysts.

Entry	Catalyst	Co wt%[a]	C wt%[b]	N wt%[b]	H wt%[b]
1	$(Co\text{-}N)_{6.78}$/NC	6.78	61.12	10.77	5.76
2	$Co/NC_{mel\text{-}f}$	6.21	72.74	5.60	2.29

a determined by ICP-AES analysis.

b determined by by CHN Elemental analysis

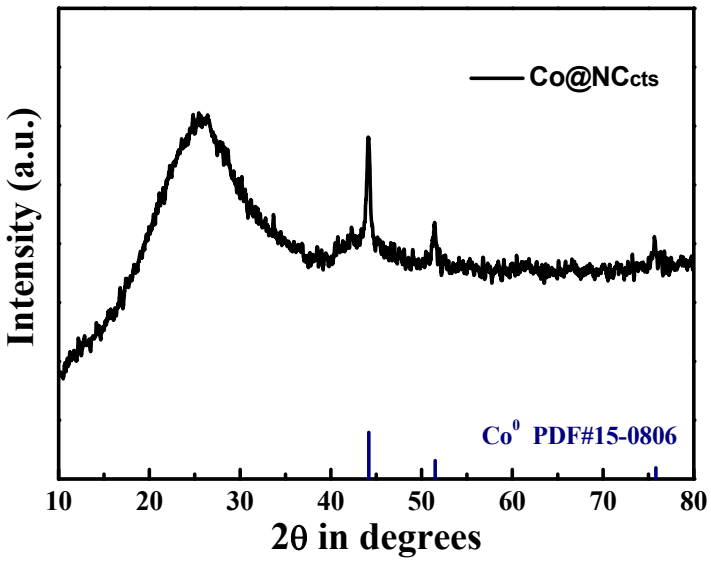

Figure S4. XRD pattern of Co@NC_{cts}

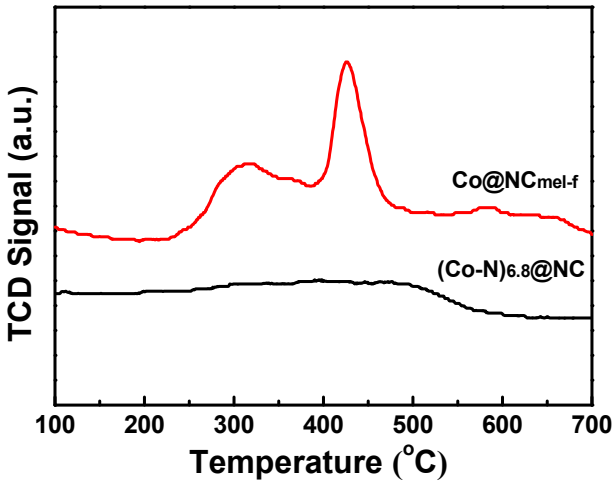

Figure S5. H_2-TPR spectra of $(Co\text{-}N)_{6.8}$@NC and Co@$NC_{mel\text{-}f}$.

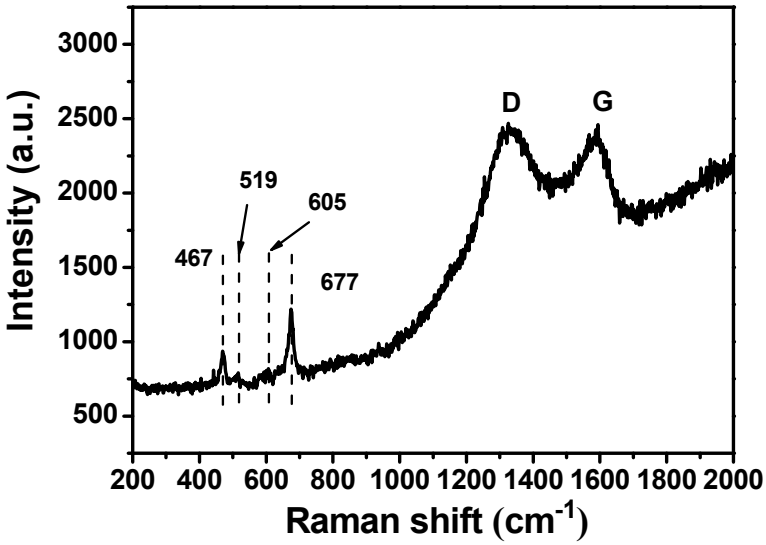

Figure S6. Raman spectrum of $(Co\text{-}N)_{6.8}$@NC washed with 0.5 M HCl.

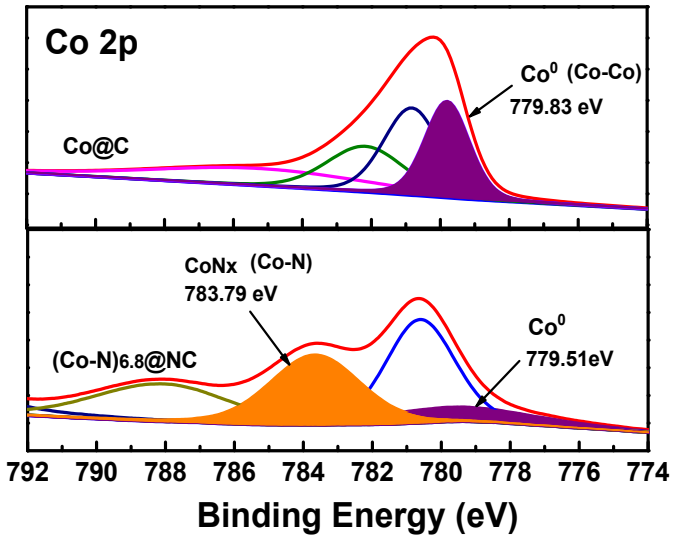

Figure S7. Co 2p XPS spectra of Co@C and $(Co\text{-}N)_{6.8}$@NC.

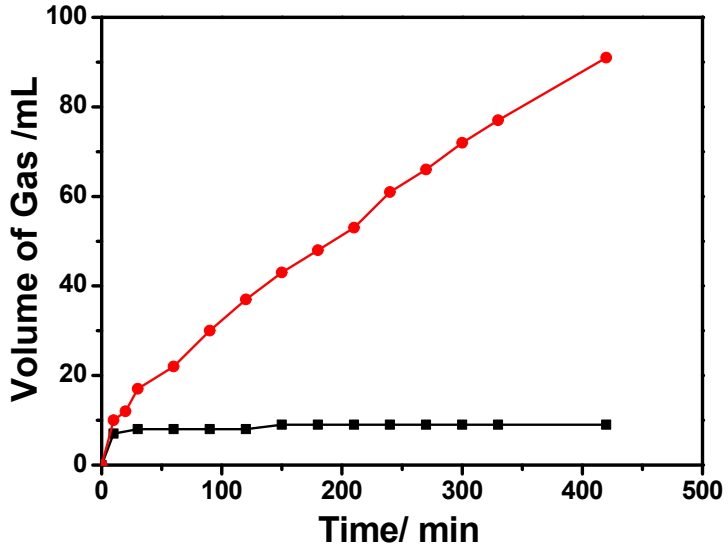

Figure S8. The results of poisoning experiment by adding KSCN into the $(Co\text{-}N)_{3.1}$@NC-containing FA dehydrogenation system.

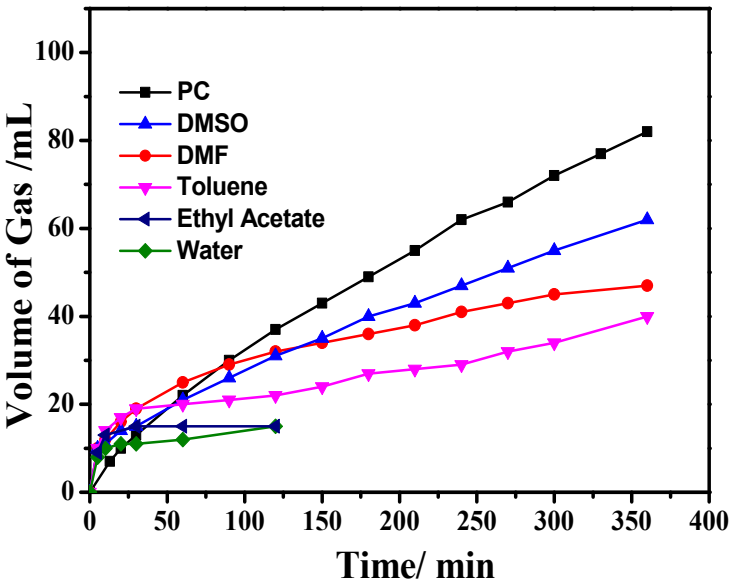

Figure S9. The effect of the solvent on the catalytic activity of $(Co\text{-}N)_{3.1}$@NC for FA dehydrogenation.

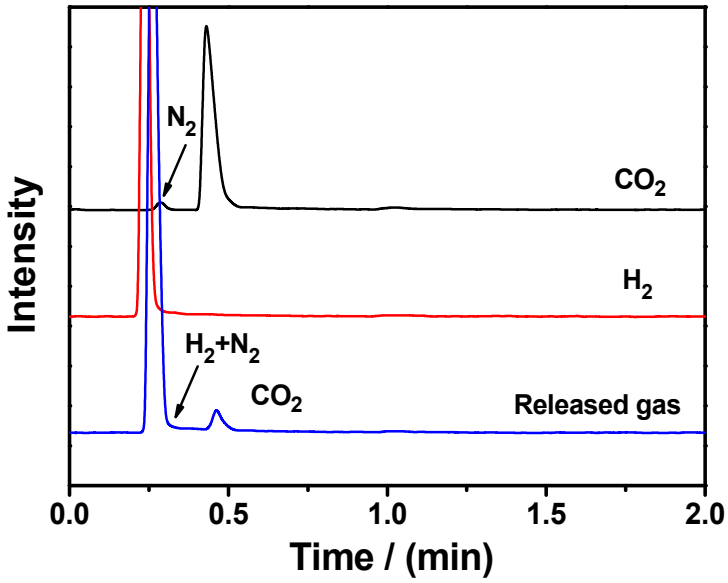

Figure S10. Gas chromatogram of the released gas form the decomposition of FA.

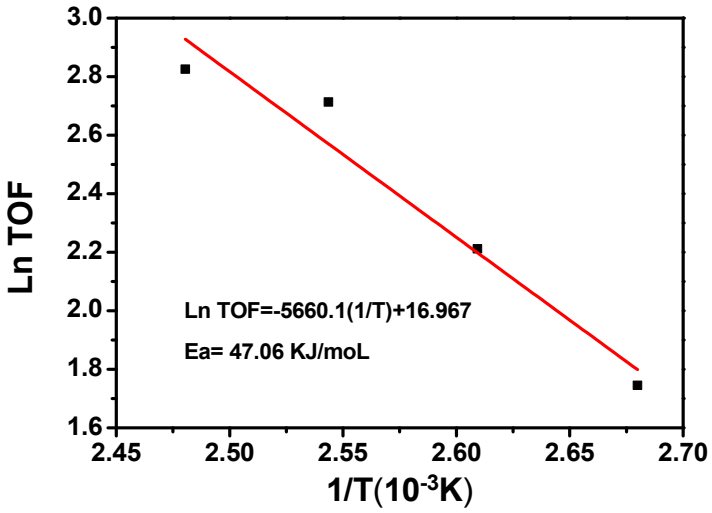

Figure S11. Arrhenius plot of the dehydrogenation of FA over $(Co\text{-}N)_{3.1}$@NC.

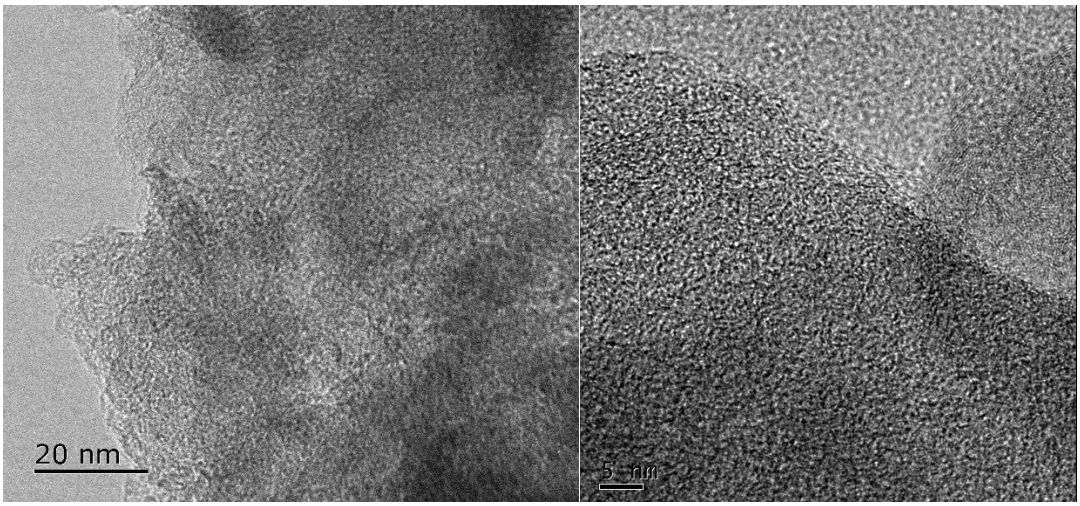

Figure S12. The HTEM images for the recovered $(Co\text{-}N)_{3.1}$@NC.

Table S2. The transfer hydrogenation of quinoline with FA over $(Co\text{-}N)_{6.8}$@NC

Entry	Amount of catalyst(mg)	Temp (^{o}C)	Time (h)	Conv. (%)[b]	Sel. (%)[c]
1	30	90	6	85	98
2	30	100	6	96	98.6
3	30	110	6	99	99
4	30	120	6	99	99
5	30	110	1	75	95
6	30	110	2	90	98
7	30	110	3	95	98
8	30	110	4	99	99
9	30	110	5	99	99
10	5	110	4	77	94
11	10	110	4	93	97
12	20	110	4	97	99
13	40	110	4	99	99

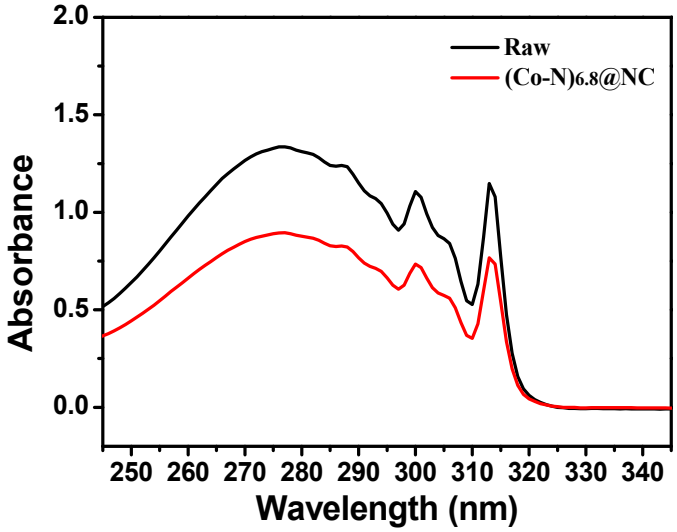

Figure S13. The UV-vis spectra of quinolone adsporption over $(Co\text{-}N)_{6.8}$@NC.

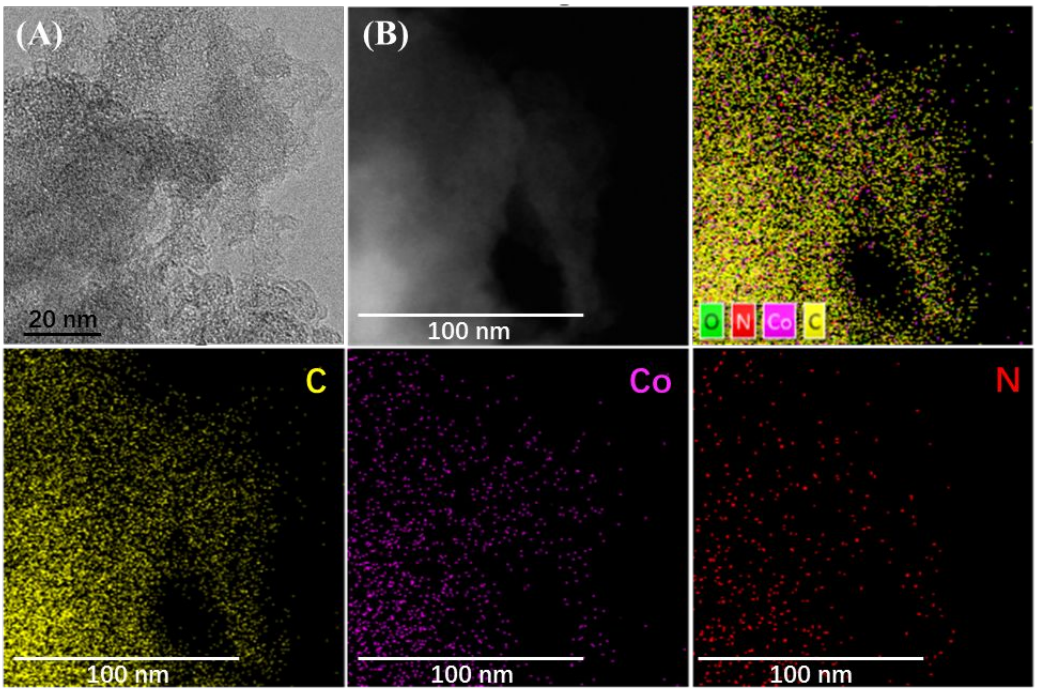

Figure S14. (A) TEM image of reused $(Co\text{-}N)_{6.8}$@NCand (B) EDS mapping images of Co in reused $(Co\text{-}N)_{6.8}$@NC.

Table S3. Selected heterogeneous catalysts for the dehydrogenation of formic acid

Entry	Catalyst	Additive FA/SF	Temp.(K)	TOF[a] (h^{-1})	Gas-production Rate [mLg^{-1}_{metal} h^{-1}]	Ref.
Only noble metal						
1	PdAuEu/C	3:1	365	387		S1
2	Ag@Pd	-	293	125		S2
3	Pd/C	1.06:0.84	298	64		S3
4	Au/ZrO_2	5:2(FA/NEt_3)	323	1590		S4
5	Au@Pd/N-mrGO		298	89	8475	S5
6	PdAg/basic resin	9:1	348	1900	360000	S6
7	Pd/NH_2-MIL-125	5:4	305	214		S7
8	Pd/mpg-C_3N_4	1:0	298	144		S8
9	Pd-B/C	11:8	303	1184[a]		S9
10	AgPd/MIL-101	-	353	848		S10
11	$Ag_{18}Pd_{82}$@ZIF-8	3:1	353	580		S11
12	Pd/S-1-in-K	1:1	323	3027		S12
13	Au@Schiff-SiO_2	1:0	323	4368		S13
14	Pd/PDA-rGO	1:1	323	3810		S14
15	$Pd/CN_{0.25}$	1:0	298	5530		S15
16	Pd^0/CeO_2	1:9	303	2040		S16
17	Pd/MSC-30	2:5	333	8414	3840000	S17
18	PdAg/amine-MSC	9:1	348	5638		S18
19	*In situ*-Pd/MSC	1:1	333	9110		S19
20	Pd@CN900K	1:3	333	14400		S20
21	Pd/PW/melem	1:1	323	15393		**S21(our previous work)**
Mixture of noble and non-noble metal						
22	$Co_{0.30}Au_{0.35}Pd_{0.35}$/C	1:0	298	80[a]	15800	S22
23	PdNi@Pd/GNs-CB	1:1	323	150[a]		S23
24	$Ni_{0.40}Au_{0.15}Pd_{0.45}$/C	-	298	12[a]		S24
25	CoAuPd/DNA-rGO	-	298	85[a]	30400	S25
26	$(Co)_6Ag_{0.1}Pd_{0.9}$/RGO	1:2.5	323	2739		S26
27	$NiPd/NH_2$-N-rGO	-	298	954		S27
Only non-noble metal						
28	Co(1)/phen(7)/C	-	383	-	19300[a]	S28
29	**$(Co\text{-}N)_{3.1}$@NC**	**-**	**393**	**-**	**16451[a]**	**This work**

[a] Initial TOF values calculated for the initial stages of the catalytic reactions.

(S1) Zhou, X.; Huang, Y.; Liu, C.; Liao, J.; Lu, T.; Xing, W. Available Hydrogen from Formic Acid Decomposed by Rare Earth Elements Promoted Pd-Au/C Catalysts at Low Temperature. *ChemSusChem* **2010**, ***3***, 1379-1382.

(S2) Tedsree, K.; Li, T.; Jones, S.; Chan, C. W. A.; Yu, K. M. K.; Bagot, P. A. J.; Marquis, E. A.; Smith, G. D. W.; Tsang, S. C. E. Hydrogen Production from Formic Acid Decomposition at Room Temperature Using a Ag-Pd Core-Shell Nanocatalyst. *Nat. Nanotech.* **2011**, *6*, 302.

(S3) Wang, Z. L.; Yan, J. M.; Wang, H. L.; Ping, Y.; Jiang, Q. Pd/C Synthesized with Citric Acid: an Efficient Catalyst for Hydrogen Generation from Formic Acid/Sodium Formate. *Sci. Rep.* **2012**, *2*, 598.

(S4) Bi, Q. Y.; Du, X. L.; Liu, Y. M.; Cao, Y.; He, H. Y.; Fan, K. N. Efficient Subnanometric Gold-Catalyzed Hydrogen Generation via Formic Acid Decomposition under Ambient Conditions. *J. Am. Chem. Soc.* **2012**, *134*, 8926-8933.

(S5) Wang, Z. L.; Yan, J. M.; Wang, H. L.; Ping, Y.; Jiang, Q. Au@Pd Core-Shell Nanoclusters Growing on Nitrogen-Doped Mildly Reduced Graphene Oxide with Enhanced Catalytic Performance for Hydrogen Generation from Formic Acid. *J. Mater. Chem. A* **2013**, *1*, 12721-12725.

(S6) Mori, K.; Dojo, M.; Yamashita, H. Pd and Pd-Ag Nanoparticles within A Macroreticular Basic Resin: an Efficient Catalyst for Hydrogen Production from Formic Acid Decomposition. A*CS Catal.* **2013**, *3*, 1114-1119.

(S7) Martis, M.; Mori, K.; Fujiwara, K.; Ahn, W. S.; Yamashita, H. Amine-Functionalized MIL-125 with Imbedded Palladium Nanoparticles as an Efficient Catalyst for Dehydrogenation of Formic Acid at Ambient Temperature. *J. Phys. Chem. C* **2013**, *117*, 22805-22810.

(S8) Lee, J. H.; Ryu, J.; Kim, J. Y.; Nam, S. W.; Han, J. H.; Lim, T. H.; Gautam, S.; Chae, K. H.; Yoon, C. W. Carbon Dioxide Mediated, Reversible Chemical Hydrogen Storage Using A Pd Nanocatalyst Supported on Mesoporous Graphitic Carbon Nitride. *J. Mater. Chem. A* **2014**, *2*, 9490-9495.

(S9) Jiang, K.; Xu, K.; Zou, S. Z.; Cai, W. B. B-Doped Pd Catalyst: Boosting Room-Temperature Hydrogen Production from Formic Acid-Formate Solutions. *J. Am. Chem. Soc.* **2014**, *136*, 4861-4864.

(S10) Dai, H. M.; Cao, N.; Yang, L.; Su, J.; Luo, W.; Cheng, G. Z. AgPd Nanoparticles Supported on MIL-101 as High Performance Catalysts for Catalytic Dehydrogenation of Formic Acid. *J. Mater. Chem. A* **2014**, *2*, 11060-11064.

(S11) Dai, H. M.; Xia, B. Q.; Wen, L.; Du, C.; Su, J.; Luo, W.; Cheng, G. Z. Synergistic Catalysis of AgPd@ZIF-8 on Dehydrogenation of Formic Acid. *Appl. Catal. B* **2015**, *165*, 57-62.

(S12) Wang, N.; Sun, Q. M.; Bai, R. S.; Li, X.; Guo, G. Q.; Yu, J. H. In situ Confinement of Ultrasmall Pd Clusters within Nanosized Silicalite-1 Zeolite for Highly Efficient Catalysis of Hydrogen Generation. *J. Am. Chem. Soc.* **2016**, *138*, 7484-7487.

(S13) Liu, Q.; Yang, X.; Huang, Y.; Xu, S.; Su, X.; Pan, X.; Xu, J.; Wang, A.; Liang, C.;

Wang, X.; Zhang, T. A Schiff Base Modified Gold Catalyst for Green and Efficient H_2 Production from Formic Acid. *Energy Environ. Sci.* **2015**, *8*, 3204-3207.

(S14) Song, F. Z.; Zhu, Q. L.; Tsumori, N.; Xu, Q. Diamine-Alkalized Reduced Graphene Oxide: Immobilization of Sub-2 nm Palladium Nanoparticles and Optimization of Catalytic Activity for Dehydrogenation of Formic Acid. *ACS Catal.* **2015**, *5*, 5141-5144.

(S15) Bi, Q. Y.; Lin, J. D.; Liu, Y. M.; He, H. Y.; Huang, F. Q.; Cao, Y. Dehydrogenation of Formic Acid at Room Temperature: Boosting Palladium Nanoparticle Efficiency by Coupling with Pyridinic-Nitrogen-Doped Carbon. *Angew. Chem., Int. Ed.* **2016**, *55*, 11849-11853.

(S16) Akbayrak, S.; Tonbul, Y.; Özkar, S. Nanoceria Supported Palladium (0) Nanoparticles: Superb Catalyst in Dehydrogenation of Formic Acid at Room Temperature. *Appl. Catal., B* **2017**, *206*, 384-392.

(S17) Li, Z. P.; Yang, X. C.; Tsumori, N.; Liu, Z.; Himeda, Y.; Autrey, T.; Xu, Q. Tandem Nitrogen Functionalization of Porous Carbon: Toward Immobilizing Highly Active Palladium Nanoclusters for Dehydrogenation of Formic Acid. *ACS Catal.* **2017**, *7*, 2720-2724.

(S18) Masuda, S.; Mori, K.; Futamura, Y.; Yamashita, H. PdAg Nanoparticles Supported on Functionalized Mesoporous Carbon: Promotional Effect of Surface Amine Groups in Reversible Hydrogen Delivery/Storage Mediated By Formic Acid/CO_2. *ACS Catal.* **2018**, *8*, 2277-2285.

(S19) Zhu, Q. L.; Song, F. Z.; Wang, Q. J.; Tsumori, N.; Himeda, Y.; Autrey, T.; Xu, Q. A Solvent-Switched in Situ Confinement Approach for Immobilizing Highly-Active Ultrafine

Palladium Nanoparticles: Boosting Catalytic Hydrogen Evolution. *J. Mater. Chem. A* **2018**, *6*, 5544-5549.

(S20) Wang, Q. J.; Tsumori, N.; Kitta, M.; Xu, Q. Fast Dehydrogenation of Formic Acid over Palladium Nanoparticles Immobilized in Nitrogen-Doped Hierarchically Porous Carbon. *ACS Catal.* **2018**, *8*, 12041-12045.

(S21) Leng, Y.; Zhang, C. J.; Liu, B.; Liu, M. M.; Jiang, P. P.; Dai, S. Synergistic Activation of Palladium Nanoparticles by Polyoxometalate-Attached Melem for Boosting Formic Acid Dehydrogenation Efficiency. *ChemSusChem* **2018**, *11*, 3396-3401.

(S22) Wang, Z. L.; Yan, J. M.; Ping, Y.; Wang, H. L.; Zheng, W. T.; Jiang, Q. An Efficient CoAuPd/C Catalyst for Hydrogen Generation from Formic Acid at Room Temperature. *Angew. Chem., Int. Ed.* **2013**, *52*, 4406-4409.

(S23) Qin, Y. l.; Wang, J.; Meng, F. Z.; Wang, L. M.; Zhang, X. B. Efficient PdNi and PdNi@Pd-Catalyzed Hydrogen Generation via Formic Acid Decomposition at Room Temperature. *Chem. Commun.* **2013**, *49*, 10028-10030.

(S24) Wang, Z. L.; Ping, Y.; Yan, J. M.; Wang, H. L.; Jiang, Q. Hydrogen Generation From Formic Acid Decomposition at Room Temperature Using a NiAuPd Alloy Nanocatalyst. *Int. J. Hydrogen Energy* **2014**, *39*, 4850-4856.

(S25) Wang, Z. L.; Wang, H. L.; Yan, J. M.; Ping, Y.; O, S.; Li, S. J.; Jiang, Q. DNA-Directed Growth of Ultrafine Coaupd Nanoparticles on Graphene as Efficient Catalysts for Formic Acid Dehydrogenation. *Chem. Commun.* **2014**, *50*, 2732-2734.

(S26) Chen, Y.; Zhu, Q. L.; Tsumori, N.; Xu, Q. Immobilizing Highly Catalytically Active Noble Metal Nanoparticles on Reduced Graphene Oxide: a Non-Noble Metal Sacrificial Approach. *J. Am. Chem. Soc.* **2015**, *137*, 106-109.

(S27) Yan, J. M.; Li, S. J.; Yi, S. S.; Wulan, B. R.; Zheng, W. T.; Jiang, Q. Anchoring and Upgrading Ultrafine NiPd on Room-Temperature-Synthesized Bifunctional NH_2-N-rGO toward Low-Cost and Highly Efficient Catalysts for Selective Formic Acid Dehydrogenation. *Adv. Mater.* **2018**, *30*, 1703038.

(S28) Tang, C. H.; Surkus, A. E.; Chen, F.; Pohl, M. M.; Agostini, G.; Schneider, M.; Junge, H.; Beller, M. A Stable Nanocobalt Catalyst with Highly Dispersed CoN_x Active Sites for the Selective Dehydrogenation of Formic Acid. *Angew. Chem., Int. Ed.* **2017**, *56*, 16616-16620.

Table S4. Comparison of transfer hydrogenation performance for quinolines of reported catalysts.

Entry	Catalyst	Temp. (° C)	Reaction time (h)	Additive	Conv.(%)	Sel.(%)	Ref.
1	Ir/SiO_2	80	24	HCOONa	100	98	S29
2	Pd/C	150	3		99	99	S30
3	Au/TiO_2-R	100	5	Et_3N	99	98	S31
4	*Co/Melamine-2@C-700*	130	18	-	100	98	S32
5	ISAS-Co/OPNC	120	1.5	-	99	99	S33
6	**$(Co\text{-}N)_{6.8}$@NC**	**110**	**4**	**-**	**99**	**99**	**This work**

(S29) Zhang, J. F.; Zhong, R.; Zhou, Q.; Hong, X.; Huang, S.; Cui, H. Z.; Hou, X. F. Recyclable Silica-Supported Iridium Catalysts for Selective Reductive Transformation of Quinolines with Formic Acid in Water. *ChemCatChem* **2017**, *9*, 2496-2505.

(S30) Kulkarni, A.; Gianatassio, R.; Török, B. Pd/C-Catalyzed Reductive Formylation of Indoles and Quinolines Using Formic Acid. *Synthesis* **2011**, *08*, 1227-1232.

(S31) Tao, L.; Zhang, Q.; Li, S. S.; Liu, X.; Liu, Y. M.; Cao, Y. Heterogeneous Gold‐Catalyzed Selective Reductive Transformation of Quinolines with Formic Acid. *Adv. Synth. Catal.* **2015**, *357*, 753-760.

(S32) Chen, F.; Sahoo, B.; Kreyenschulte, C.; Lund, H.; Zeng, M.; He, L.; Junge, K.; Beller, M. Selective Cobalt Nanoparticles for Catalytic Transfer Hydrogenation of N-Heteroarenes. *Chem. Sci.* **2017**, *8*, 6239-6246.

(S33) Han, Y. H.; Wang, Z. Y.; Xu, R. R.; Zhang, W.; Chen, W. X.; Zheng, L. R.; Zhang, J.; Luo, J.; Wu, K. L.; Zhu, Y. Q.; Chen, C.; Peng, Q.; Liu, Q.; Hu, P.; Wang, D. S.; Li, Y. D. Ordered Porous Nitrogen-Doped Carbon Matrix with Atomically Dispersed Cobalt Sites as an Efficient Catalyst for Dehydrogenation and Transfer Hydrogenation of N-Heterocycles. *Angew. Chem. Int. Ed.* **2018**, *57*, 11262-11266.

Analytical Data of the Obtained Compounds

GC-MS:

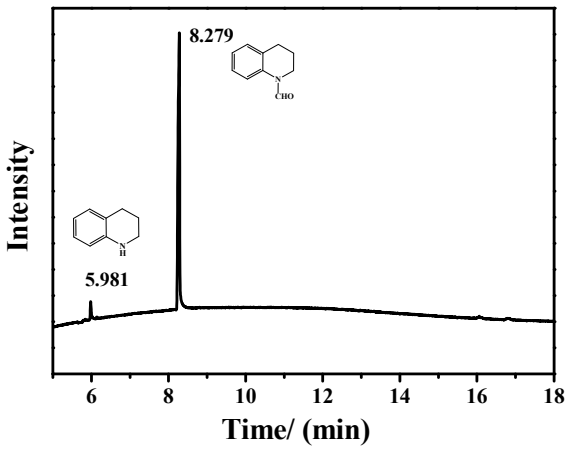

Figure S15. GC-MS chromatogram of the reaction mixture form the transfer hydrogenation of quinoline

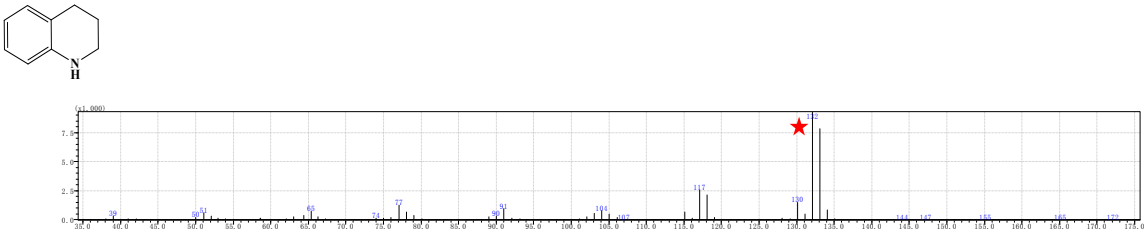

Figure S16. Mass Spectra of 1,2,3,4-tetrahydroquinoline

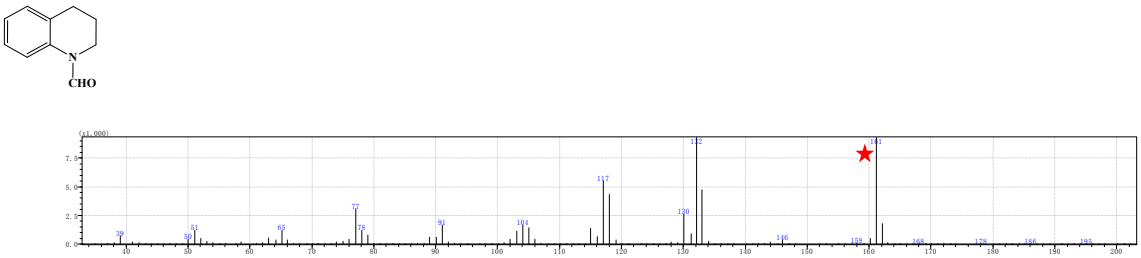

Figure S17. Mass Spectra of 3,4-dihydroquinoline-1(2H)-carbaldehyde

NMR Spectra of the Obtained Compounds

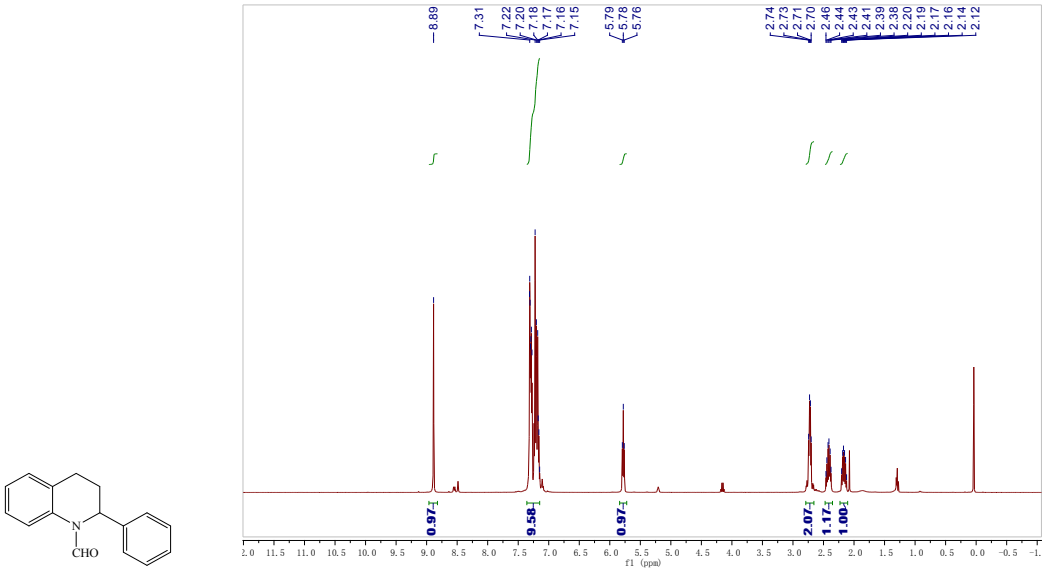

^{1}H NMR (400 MHz, $CDCl_3$) δ 8.89 (s, 1H), 7.36 – 7.14 (m, 9H), 5.78 (t, *J* = 6.3 Hz, 1H), 2.79 – 2.66 (m, 2H), 2.47 – 2.35 (m, 1H), 2.23 – 2.10 (m, 1H).

Figure S18. 1H- NMR spectrum of formamide product of 2-benzylquinoline

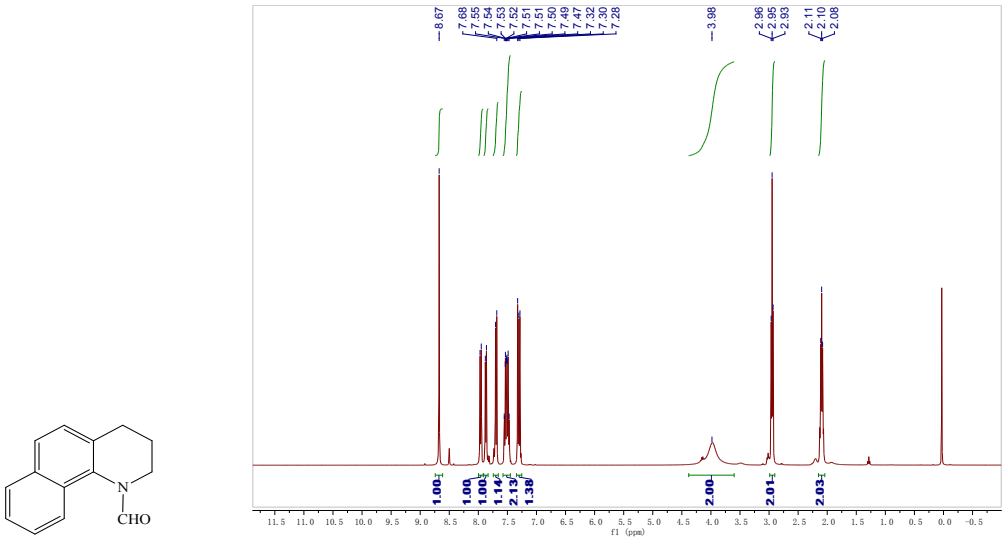

^{1}H NMR (400 MHz, $CDCl_3$) δ 8.67 (s, 1H), 7.96 (d, *J* = 8.3 Hz, 1H), 7.87 (d, *J* = 7.6 Hz, 1H), 7.69 (d, *J* = 8.3 Hz, 1H), 7.57 – 7.45 (m, 2H), 7.35 – 7.26 (m, 1H), 4.11 (brs, 2H), 2.95 (t, *J* = 6.7 Hz, 2H), 2.16 – 2.04 (m, 2H).

Figure S19. 1H- NMR spectrum of formamide product of 7,8-benzoquinoline

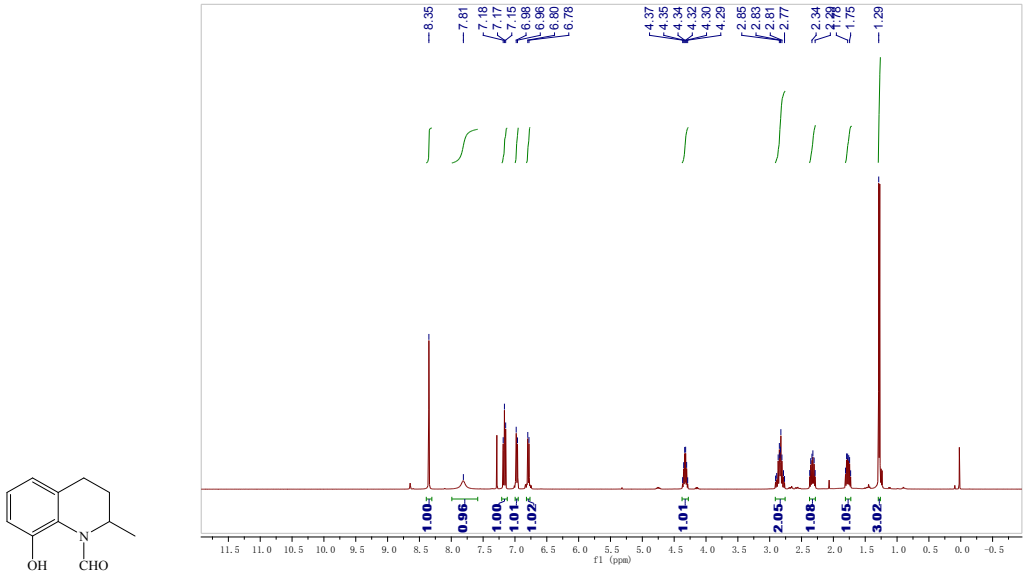

^{1}H NMR (400 MHz, $CDCl_3$) δ = 8.35 (s, 1H), 7.81 (s, 1H), 7.21 – 7.12 (m, 1H), 6.97 (d, *J*=8.1, 1H), 6.79 (d, *J*=7.5, 1H), 4.40 – 4.23 (m, 1H), 2.89 – 2.74 (m, 2H), 2.33 (dt, *J*=14.1, 6.3, 1H), 1.77 (dt, *J*=12.0, 6.5, 1H), 1.29 (d, 3H).

Figure S20. 1H- NMR spectrum of formamide product of 8-hydroxyquinaldine

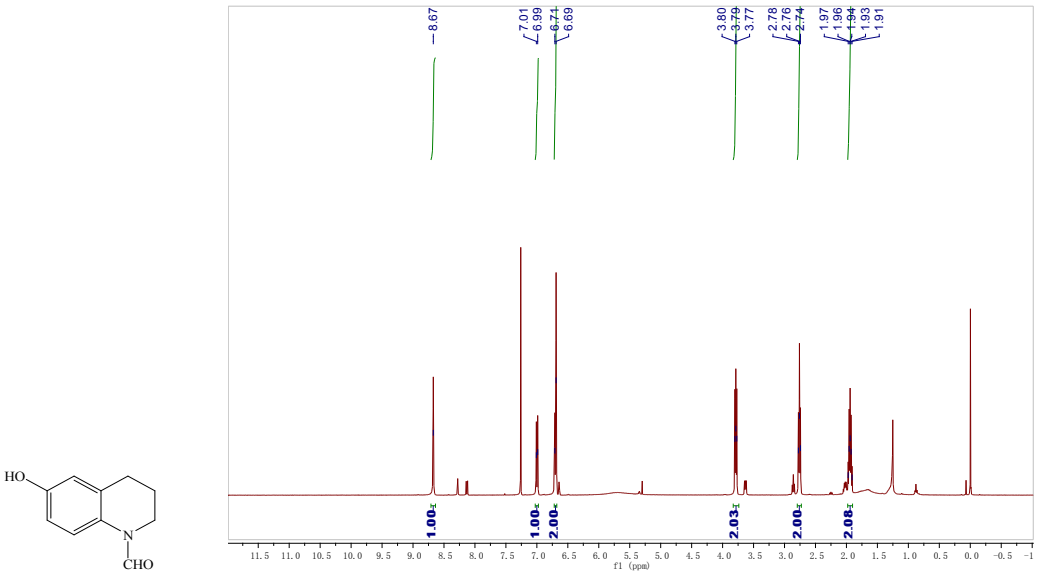

^{1}H NMR (400 MHz, $CDCl_3$) δ 8.67 (s, 1H), 7.00 (d, J = 8.5 Hz, 1H), 6.70 (d, J = 8.0 Hz, 2H), 3.82 – 3.75 (m, 2H), 2.76 (t, J = 6.5 Hz, 2H), 2.03 – 1.87 (m, J = 12.6, 6.4 Hz, 2H).

Figure S21. 1H- NMR spectrum of 6-hydroxyquinoline